

Superconductivity, Fermi-liquid transport, and universal kinematic scaling relation for metallic thin films with stabilized defect complexes

M. ElMassalami^{*} and M. B. Silva Neto[†]*Instituto de Física, Universidade Federal do Rio de Janeiro, Caixa Postal 68528, 21941-972 Rio de Janeiro RJ, Brazil*

(Received 15 February 2021; revised 23 June 2021; accepted 6 July 2021; published 27 July 2021)

Detailed analysis reveals that an incorporation of stabilized defect complexes within metallic thin films, though a highly disordering and nonequilibrium process, gives rise to superconductivity, Fermi-liquid (FL) transport, and a universal correlation among them. This remarkable manifestation of correlated macroscopic quantum effects is attributed to a phonon-mediated electron-electron, e-e, scattering channel which encompasses both Koshino-Taylor and Bergmann's pseudo-Umklapp processes. This channel—denoted below as pseudo-Umklapp e-e scattering channel—is distinctly different from traditional ones in that disorder leads to a breakdown of lattice momentum conservation (significantly enlarging available phase space), to a spectral weight transfer towards lower frequencies (modifying electron-phonon coupling constant λ), and to a relaxation of kinematic constraints (all phonic polarization modes become available for mediation). On modeling the distorted structure in terms of Hosemann's paracrystal and using standard quantum many-body techniques, we demonstrate the role of distortion and softening in establishing this pseudo-Umklapp channel and, consequently, the surge of superconductivity, the FL transport, and the correlation of their parameters. This unifying approach allows us to derive analytical expressions for $T_c(\rho_o)$ (hallmark of superconductivity), the coefficient $A(\rho_o)$ (hallmark of FL transport), and the universal kinematic scaling relation $\ln(\frac{T_c}{\theta}) \propto A^{-\frac{1}{2}}$: All are in satisfactory agreement with experiments (θ is an energy scale; residual resistivity ρ_o measures the extent of disorder).

DOI: [10.1103/PhysRevB.104.014520](https://doi.org/10.1103/PhysRevB.104.014520)

I. INTRODUCTION

Real crystalline solids do not exhibit a perfectly ordered atomic arrangement; rather, some degree of imperfection, Fig. 1(a), is always present in the form of naturally occurring or artificially engineered defects [1]. Manipulation of the type, concentration, and distribution of these defects can be exploited for effecting a dramatic variation in the mechanical, thermal, optical, and electronic properties. Such a manipulation is extensively employed for engineering highly desirable technological or scientific marvels, such as stainless steel, semiconductor electronic components, and high-temperature superconductors.

Here we are interested in the influence of defect incorporation on the electric transport properties. We consider the introduction, under well specified and controlled conditions, of a defective substructure within a metallic or semiconducting target which can be in the form of a bulk or a thin film. A variety of techniques can be used for such defect incorporation, e.g., ion bombardment (implantation [2–7] or irradiation [8]), particles bombardment (e.g., electrons [9], neutron [9], proton [10]), co-sputtering [11,12], co-evaporation [13–16], laser irradiation [17], or (vapor, liquid) quench condensation [14,17,18]. The evolution of the electric transport with defect incorporation is usually monitored by *in situ* or *ex situ* probes such as electrical resistivity [4,15,19–21] (the only property to be considered

here). A vast body of data on the evolution of resistivity with defect incorporation has been collected during the last seven decades. A detailed analysis of these data indicates that, under certain conditions, defect incorporation leads to a surge of macroscopic quantum phenomena [namely superconductivity and Fermi-liquid (FL) states] and that the evolution of, and correlations among, these effects are strongly controlled by the type and extent of incorporated defects.

These important findings can be illustrated by considering defect incorporation within an aluminium [4,6–8,11,16,22,23] (or tin [2,14,22,24–26]) thin film. An Al film, less than 1 μm thick and free of intentionally incorporated defects, exhibits a small residual resistivity, $\rho_o \leq 10 \mu\Omega \text{cm}$, low superconducting transition temperature, $T_c \simeq 1.2 \text{ K}$, and a temperature-dependent resistivity consisting of a dominant Bloch-Grüneisen βT^5 term and a negligible electron-electron, e-e, AT^2 contribution, $A \simeq 10^{-7} \mu\Omega \text{cm/K}^2$. Incorporation of a few percents of defects (e.g., implanted O, Si, Ge, H, or even Al) gives rise to [4–8,11,16,22,23] (i) an increase in ρ_o ($10 \mu\Omega \text{cm} \rightarrow 10^4 \mu\Omega \text{cm}$), (ii) an enhancement [27] in T_c ($1 \text{ K} \rightarrow 8.4 \text{ K}$) [6,7,11,16], and (iii) a surge of a robust A ($10^{-7} \mu\Omega \text{cm/K}^2 \rightarrow \mu\Omega \text{cm/K}^2$) [28]. These influences were attributed to stabilized defect complexes since their reduction by annealing minimizes or even eliminates these features [4,8,29,30].

These defect-incorporation-related features, observed in a variety of conventional superconductors, are impressive, unexpected, and quite puzzling. Consider the following three arguments (for details and references, see below): First, although Anderson's theorem [31] predicts no change in T_c when nonmagnetic defects are incorporated, yet experiments

^{*}massalam@if.ufrj.br[†]mbsn@if.ufrj.br

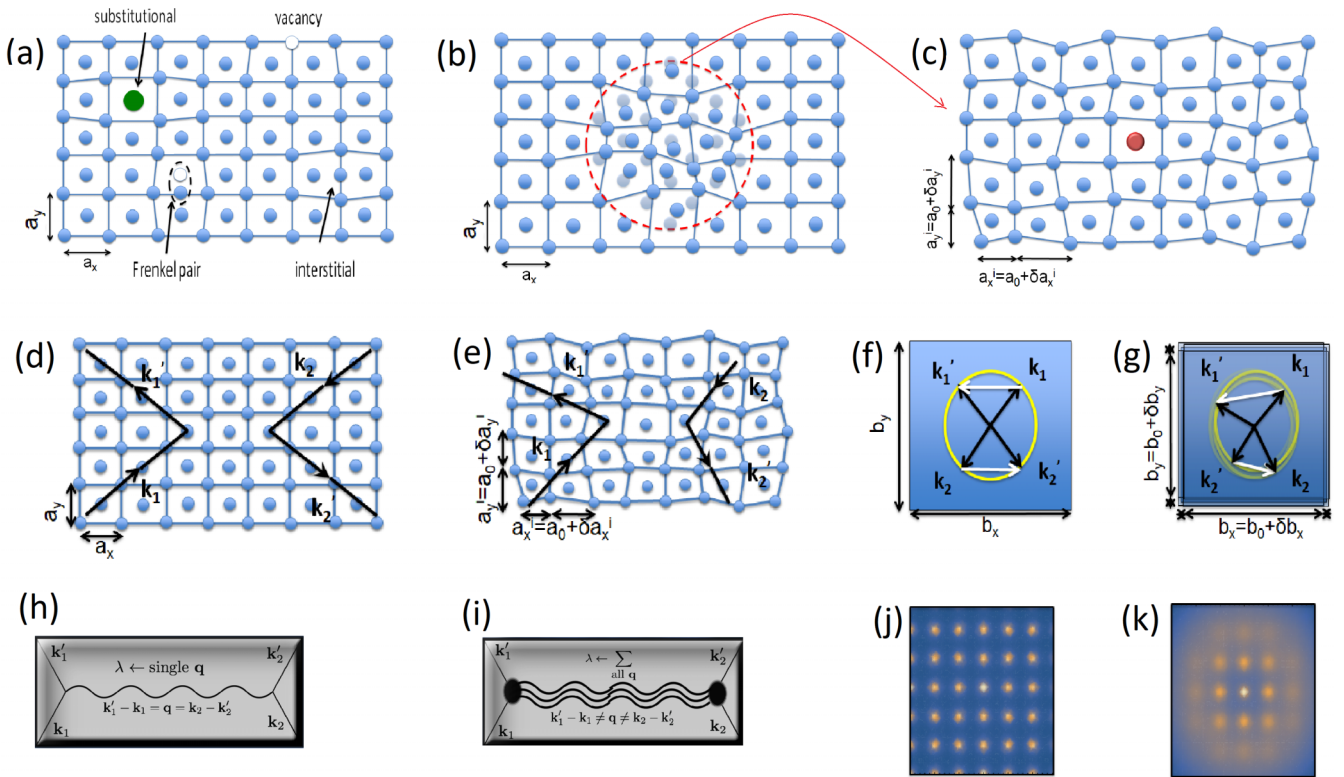


FIG. 1. Defectual description and implication. (a) Examples of point defects in a crystalline solid; (b) a sketch of agglomerated defects (represented as a sphere with a radius $nm < D < \mu m$) arising after, e.g., implantation/irradiation with heavy ions effected at low temperature [17]: As diffusion is extremely hindered, this leads to a frozen-in of a nano-sized agglomerate (labeled here as *defectal*) within an otherwise perfect crystal. (c) Modelling of a defectal-bearing crystal in terms of a distorted lattice plus a heavy, Lifshitz-type scatterer. The curved arrow suggests that panel (c) is an extension of defectal structure of panel (b) to the whole crystal: a valid approximation whenever the mean free path and coherence length are much shorter than D . Effective e-e scattering process occurring within a pristine (d) and distorted (e) direct lattices. The same e-e process within the first Brillouin zone of pristine (f) and distorted (g) reciprocal lattices; similarly, in terms of Feynman diagrams for the pristine (h) and distorted (i) cases. The Fraunhofer diffraction pattern for pristine (j) and distorted (k) structures, in which a typical amorphization halo is observed at higher-order reciprocal lattice points [18].

indicate a strongly modified T_c . Second, it is recalled that the phase space available for momentum relaxation is severely limited by lattice momentum conservation and, accordingly, one expects a negligibly small A [32]; yet, experiments demonstrate a dominant AT^2 FL contribution. Finally, it is expected that ρ_o is determined by the electron-impurity scattering ($\rho_o \sim |V_{imp}|^2$) that $T_c \sim e^{-1/\lambda}$ is associated with electron-phonon coupling ($\lambda \sim |V_{ep}|^2$), and that A is determined by e-e interaction ($A \sim |V_{ee}|^2$). Accordingly, one expects ρ_o , T_c , and A to be independent [33]; yet, experiments reveal that T_c and A are markedly correlated with each other as well as with ρ_o .

Various theoretical investigations analyzed the surge of such disorder-driven features (see, e.g., Refs. [18,30,34–40] and references therein). These analyses considered such features to be driven by separate causes; accordingly, no correlation or scaling were established among their parameters. As an illustration, the disorder-driven trend of T_c was attributed to an additional phonon-mediated e-e scattering process [18,30,34] while, on the other hand, the surge and evolution of defect-driven AT^2 contribution is either not considered or implicitly attributed to a Koshino-Taylor-type scattering process [38,39]. Surprisingly, no unification of

these two effects was attempted even though both analyses employed similar physical insight and quantum many-body techniques and, moreover, both considered disorder as being due to a set of nonagglomerated defects.

This work, while bearing some resemblance to Refs. [18,30,38,39], adopts an alternative empirical and theoretical approach that treats superconductivity, FL transport, and their correlation as being driven by a multiply-polarized, phonon-mediated e-e scattering channel, operating within a region of stabilized agglomeration of defects which we consider, in contrast to previous studies, to be similar to those in Figs. 1(b) and 1(c) rather than to a collection of isolated impurities as in Fig. 1(a).

Below in Sec. II, we first survey, classify, and rationalize a vast body of empirical data; representatives were drawn from a variety of defect-bearing conventional (and less conventional) superconductors. Then, from there we extract empirical expressions that identify and correlate the evolution of the superconducting and the FL properties. Secondly, in Sec. III and Supplemental Material (SM) [41], we model the distorted structure in terms of Hosemann's paracrystalline lattice [42,43]. Employing standard theories of Migdal-Eliashberg (superconductivity) and Boltzmann

(transport), we highlight the emergence of the pseudo-Umklapp scattering channel and show how it is responsible for the surge of superconductivity, FL character, and their correlation. Based on this unified analysis, we derive analytic expressions—most importantly a universal kinematic scaling of $T_c(\rho_o)$ and $A(\rho_o)$ —that reproduce the experimental observations as well as the main conclusions of Refs. [18,30].

II. EMPIRICAL ANALYSIS: DESCRIPTION AND IMPLICATIONS OF DEFECTAL

Based on the above considerations, the low-temperature resistivity, after subtracting the lattice contribution from the total resistivity ρ_{tot} , can be simplified as

$$\rho(T) = \rho_{\text{tot}}(T) - \beta T^5 = \Theta(T - T_c)[\rho_o + AT^2], \quad (1)$$

wherein $\Theta(T - T_c) = 1(0)$ for $T > (<) T_c$. Moreover, ρ_o , T_c , and A were found to be uniquely correlated. As well illustrated for defect-bearing Al or Sn thin-film cases, such features appear only when certain types of agglomerated defects are stabilized [8,21,44,45]. These large-sized agglomerations can be created by any of the above-cited defect-incorporating processes. Moreover, these disturbances can be stabilized by certain incorporated active anchors or pinning centers (e.g., oxygen, nitrogen) [8,21,45]. Each individual agglomerate, labeled as a *defectal*, can be thought of as a three-dimensional disordered metallic region, idealized in Fig. 1(b) as a sphere of agglomerated defects, which is embedded in an otherwise perfectly arranged host. A defectal is a generalization of the term ‘‘oxygen-stabilized defect-complexes’’ coined and used in Ref. [8] for describing the disorder in the self-ion irradiated Al films.

We envisage an e-e scattering channel, see Figs. 1(d)–1(i), to be operating within the defectal space and that such a channel leads, see Secs. II A and II C, to the surge and correlation of $T_c(\rho_o)$ and $A(\rho_o)$. This channel is denoted as *pseudo-Umklapp electron-electron scattering process*; a name coined by Bergmann [30] who was the first to recognize its crucial role in disordered and amorphous superconductors (but no extension to FL transport was attempted).

Usually, ρ_o is taken to be a measure of disorder. But, in theoretical analysis, the extent of disorder is often gauged by the effective mean-free path, $\ell \propto \frac{1}{\rho_o}$ [26]: a scaling length that interpolates between the initial, before intentional incorporation, limit (marked by ℓ_o° and ρ_o°) and the amorphous limit (whereat $\rho_o \rightarrow \rho_o^{\text{am}}$ as, via Ioffe-Regel limit, $\ell \rightarrow \ell_{\text{am}} \equiv a_o$, the distance between neighboring atoms). Taking $\delta\ell \equiv 1/(\frac{1}{\ell} - \frac{1}{\ell_o^\circ})$, we obtain

$$\frac{\delta\ell}{\ell_n} = \frac{\rho_o^\circ}{\delta\rho_o}, \quad (2)$$

with $\ell_n = a_o(\frac{\rho_o^{\text{am}}}{\rho_o^\circ} - 1)$ and $\rho_o^{\text{am}} \gg \rho_o^\circ$.

A. Correlation of T_c and ρ_o

The empirical correlation among T_c and ρ_o is shown in Fig. 2 as $\frac{T_c - T_c^\circ}{T_c^\circ}$ vs $\frac{\rho_o - \rho_o^\circ}{\rho_o^\circ}$ curves for representative defectal-incorporated superconductors. Here, ρ_o° and T_c° represent some initial values, often not the pristine but the ones just

before the controlled defect incorporation. As such, $\delta\rho_o \equiv \rho_o - \rho_o^\circ$ ($\approx \rho_o$ for small ρ_o°) is a measure of the extent of the intentionally introduced defectals.

Figure 2 indicates that, in spite of such an extensive list of different materials that had been subjected to different disordering techniques, the evolution of $\frac{\delta T_c}{T_c^\circ}$ vs $\frac{\delta\rho_o}{\rho_o^\circ}$ can be grouped into the following four broad disordered classes (represented by the four quadrants of Fig. 2): (i) weak-coupled superconductors [15,29] (first quadrant); (ii) strong-coupled superconductors [15,29] (fourth quadrant); (iii) semiconducting-based distortion-bearing superconductors [46] (second quadrant); (iv) nonconventional superconductors [47] (third quadrant). In this work, we concentrate only on the properties of the two defectal-bearing conventional superconductors (first and fourth quadrants). It is emphasized that the above mentioned broad classification, in particular into weak and strong coupled superconductors, is intended for convenience of discussion. As we will see in Sec. III C, the defectal incorporation in conventional superconductors can be seen as promoting the running towards either the weak- or strong-coupling limit depending on the initial properties of the starting system.

1. Defectal-bearing weakly-coupled superconductors

Figures 2(b) and 2(c) show the $T_c(\rho_o)$ correlation in In [2,22,24,26,48], Zn [22], Ga [22,45], Al₂Au [22], AuIn₂ [22], Sn [26], and Al [8,22]. Various other weakly-coupled superconductors (e.g., simple metals Be, Zn, Cd, Sn) [22,25] can be added to this list. All exhibit a common property: defectal incorporation leads to an *enhancement* [29] of T_c and ρ_o (linear for small $\delta\rho_o$: $\delta T_c \propto \delta\rho_o$) with a slope that depends solely on material properties [see the red line in Figs. 2(c)]. The surge of $T_c(\rho_o)$ correlation in self-ion irradiated aluminum film, Fig. 2(c), indicates that the chemical character of the bombarding projectiles is not essential for defectal formation and stabilization.

2. Defectal-bearing strongly-coupled superconductors

Figures 2(d) and 2(e) show the $T_c(\rho_o)$ correlation in V₃Si [3], Nb [21,49], Nb₃Ge [20], V₃Si [3,50], V₃Ge [20], Pb [22], and Pb_{1-x}Ge_x ($x = 0.3, 0.7$) [51]. In this class, defectal incorporation leads to a *reduction in T_c* together with an increase in ρ_o [29]. This very same correlation was evident in Nb-Ti superconducting alloy [52], hydrogenated Pd [44,53], and solid-solution Pd-X (X =noble metal) [54] (interestingly, Pd is a nonsuperconducting metal in the pure state). A common property of this class is the *nonlinear character* of $\delta T_c(\delta\rho_o)$ (for all $\delta\rho_o \geq 0$) and the negative derivative, $d(\delta T_c)/d(\delta\rho_o) < 0$. Finally, it is worth mentioning that, for the superconducting binary alloys such as A_{1-x}B_x, the paraboliclike $\delta T_c(\delta\rho_o)$ behavior, Fig. 2(e), is related to the nonmonotonic evolution of $\rho_o(x)$ as dictated by Nordheim’s rule $\rho_o(x) \propto x(1-x)$.

B. Correlation of A and ρ_o

In addition to $T_c(\rho_o)$, defectal-incorporation leads to a concomitant change in $A(\rho_o)$. As an illustration,

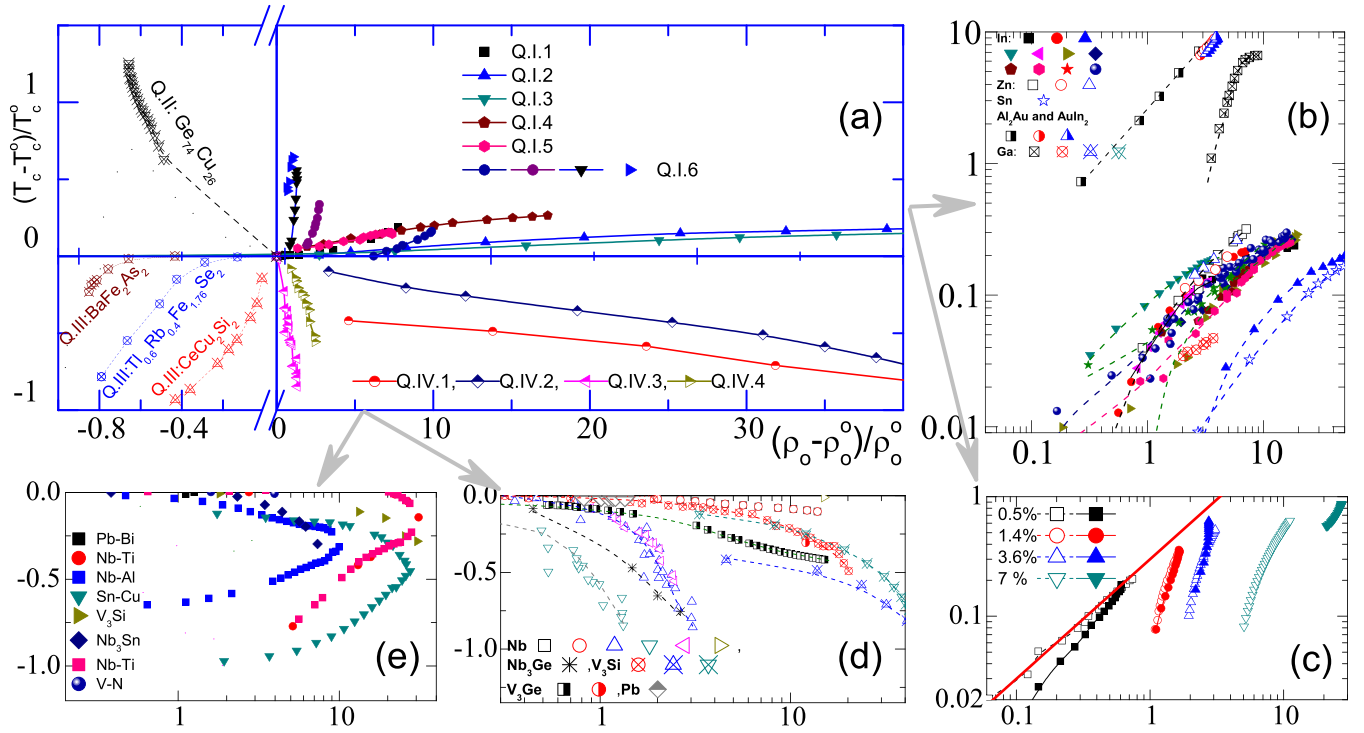


FIG. 2. Correlation of T_c and ρ_o . (a) Evolution of $\frac{\delta T_c}{T_c^0}$ vs $\frac{\delta \rho_o}{\rho_o^0}$ for representative defectal-bearing superconductors (note the scale break in the x axis). This plot, emphasizing only the excess due to the pseudo-Umklapp channel, is an improvement on earlier $T_c(\rho)$ plots reported in, e.g., Refs. [4,24,26]. Weak-coupled (first quadrant): Q.I.1: Al and O co-deposition [55], Q.I.2: indium-granular film [26], Q.I.3: Sn - granular [26], Q.I.4: In-Ar-irradiated [24], Q.I.5: In-Ar-implanted [24], Q.I.6: O-incorporated Al with Al irradiation [8]. Strong-coupled (fourth quadrant): Q.IV.1: V_3Si Kr-irradiated [3], Q.IV.2: V_3Si He-irradiated [3], Q.IV.3: Nb N-implanted [21], Q.IV.4: Nb Ne-irradiated [21]. Additional curves on defect-bearing A-15 superconductors were reported in, e.g., Refs. [20,50,56–58]. To illustrate the generality of our analysis, we select two additional classes of superconductors, namely, the semiconducting quenched-condensed class within the second quadrant (e.g., $Ge_{74}Cu_{26}$ alloys after Cu irradiation [46]) and the nonconventional superconductors class within the third quadrant, namely pnictide $BaFe_2As_2$ [59,60], chalcogenide $Tl_{0.6}Rb_{0.4}Fe_{1.76}Se_2$ [60,61], and heavy-fermion $CeCu_2Si_2$ [47,62]. (b) log-log plots of irradiated/implanted thin-films of weakly-coupled conventional BCS superconductors: In [2,22,24,26,48], Zn [22], Ga [22,45], Al_2Au [22], $AuIn_2$ [22], and Sn [26]. (c) Log-log plots of self-ion irradiation of pure (empty symbols) and granular (filled symbols) thin films of aluminum with varying concentration of defectal-stabilizing oxygen ($\leq 7\%$) [8,22]. (d) Semilog plots of the strong-coupled conventional BCS superconductors: Nb [21,49], Nb_3Ge [20], V_3Si [3,50], V_3Ge [20], Pb [22], and $Pb_{1-x}Ge_x$ ($x = 0.3, 0.7$) [51]. (e) Semilog plot of irradiated/implanted thin films of strong-coupled conventional BCS superconductors [52]. For more details, see text.

Figs. 3(a1)–3(a10), 3(b1)–3(b3) show the defectal-induced evolution of T_c , A , and ρ_o of strong-coupled V_3Si superconductor and weak-coupled In superconductor. Neutron-irradiation-induced defectal incorporation in V_3Si [Figs. 3(a5), 3(a6), and 3(a7)] leads to a surge of AT^2 contribution [Figs. 3(a1), 3(a2), 3(a3), 3(a4)] with A being strongly correlated to ρ_o [Fig. 3(a8)], to a reduction in $T_c(\rho_o)$ [Fig. 3(a5)], and to a correlation between T_c and A [Fig. 3(a10)] [9]. Similar features are evident for ion implantation in In thin films [Figs. 3(b1), 3(b2), 3(b3)] [2]. As a further illustration of defectal-incorporation induced effects, alloying into a strong-coupled superconductor [52] was shown to induce an increase in ρ_o , a change in T_c , and a switching of the T^n ($n = 3-5$) behavior into a T^2 contribution.

Unfortunately, except for a few reports—such as in Refs. [2,9,52]—the $A(\rho_o)$ correlation had not been highly appreciated nor extensively explored. As such, there are no extensive reports from which one can construct a universal $\frac{A-A_0}{A_0}$ vs $\frac{\rho_o - \rho_o^0}{\rho_o^0}$ plot. Nevertheless, for weak ρ_o , the following

empirical dependence

$$A(\rho_o) = A_0 + A_1\rho_o + A_2\rho_o^2, \quad (3)$$

can be readily identified when examining the evolution of $A(\rho_o)$ in the representative defectal-bearing strong-coupled [Fig. 3(a8)] and weak-coupled [Fig. 3(b1)] superconductors.

C. Correlation of T_c and A

Figure 3(c) reveals a remarkable BCS-like, $T_c = \theta e^{-F/\sqrt{A}}$, expression wherein θ and F are material-dependent parameters. Similarly, $\ln(\frac{T_c}{\theta}) \propto (\frac{-1}{\sqrt{A}})$, as shown in Figs. 3(a10) and 3(b3), describes reasonably well the data of the representative (weak- and strong-coupled) superconductors. In fact this is a universal scaling; it is also evident in pnictides [60], chalcogenides [63], and heavy fermion [47] superconductors. It was previously recognized and theoretically approached in, e.g., Refs. [52,64,65]; below, in contrast to these pioneering works, we attribute its surge to the pseudo-Umklapp scattering channel.

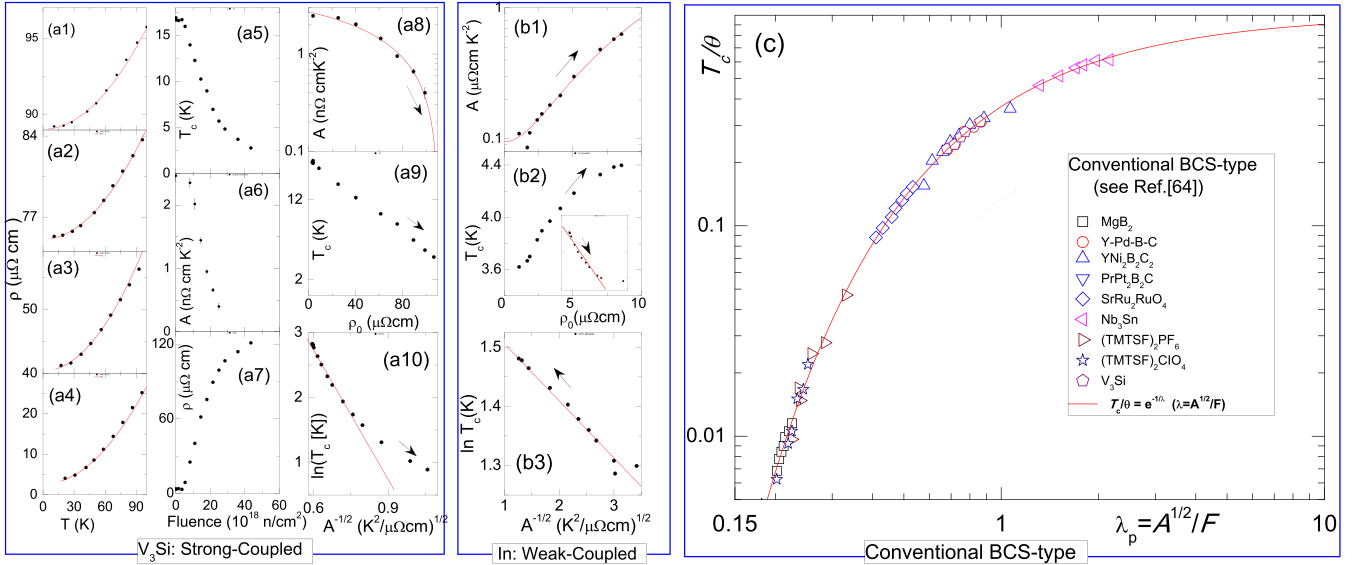


FIG. 3. Correlation of $T_c(\rho_o)$ and $A(\rho_o)$. (a) Bulk single-crystal V_3Si subjected to irradiation by neutron flux (data taken from Ref. [9]). (a1) 21.5×10^{18} n/cm², (a2) 18×10^{18} n/cm², (a3) 11×10^{18} n/cm², and (a4) 0 n/cm². The red lines are fit to $\rho_{tot}(T) = \rho_o + \beta T^5 + AT^2$. (a5) T_c vs fluence, (a6) A vs fluence, and (a7) ρ_o vs fluence. (a8) A vs ρ_o , (a9) T_c vs ρ_o , and (a10) $\ln(T_c)$ vs $A^{-1/2}$; (b) thin films of In deposited at 200 K and annealed at 300 K; afterwards implanted with In^+ ions at 2 K (data taken from Ref. [2]): (b1) A vs ρ_o , (b2) T_c vs ρ_o . Inset: $\ln T_c$ vs ρ_o^{-1} , and (b3) $\ln(T_c)$ vs $A^{-1/2}$. (c) Universal kinematic correlation between T_c and A for several weakly- and strongly- coupled BCS superconductors (data taken from Ref. [64]).

III. THEORETICAL ANALYSIS

A. The mechanism: Distortion and softening

As evident from above, defectual-incorporation modifies significantly the superconducting and FL transport properties. Below, we explore theoretically how such changes emerge. We start by modeling a defectual, see Fig. 1(b), in terms of a *distorted lattice plus a heavy scatterer*. Despite its simplicity, the structural representation of Fig. 1(c) embodies the two most important consequences of defectual-incorporation: distortion and softening. Next, we show that these combined effects trigger the surge of the pseudo-Umklapp e-e scattering process and as a consequence the superconductivity, the FL transport and their correlation.

1. Distortion: Hosemann's paracrystal

For describing the distorted structure in terms of a Hosemann's paracrystal [42], we start by assuming, for simplicity, a defectual-free cubic structure with primitive unit-cell vectors $|\mathbf{a}_{i=1,2,3}| = a_o$. Then, on an introduction of a defectual, such a cubic structure would be modified as, say, in Fig. 1(b). We consider that, due to the very same distortion, the mean free path as well as the coherence length are much smaller than the diameter of the distortion. Then, as far as the scattering events are concerned, the distortion can be extended to the whole crystal. Let us describe such an extended distortion in terms of the modified cubic structure of Fig. 1(c), wherein the new "unit vectors" vary in length and direction from cell to cell but nevertheless can still be organized in "rows and columns." We consider a Gaussian statistical probability distribution [30,42] in which the average $|\overline{\mathbf{a}}_{i=1,2,3}| = a_o$ corresponds to the center of the distribution, while the extent of distortion is given by

the width $\sigma_{ij} = \overline{\Delta a_j / \overline{a_j}}$ [42]. For simplicity, we consider equal variance, $\sigma_{ij} = \sigma \delta_{ij}$ [66].

It is recalled that for defectual-free long-range ordered crystal, Bragg reflections occur at reciprocal lattice points, $\mathbf{g}(h, k, l) = h\mathbf{b}_1 + k\mathbf{b}_2 + l\mathbf{b}_3$. However, for defectual-bearing structures, the amplitude of "Bragg reflections" is steadily decreased, while the linewidth $\delta\mathbf{g}$ at $\mathbf{g}(h, k, l)$ is monotonically broadened [42]: Fig. 1(k) shows the Fraunhofer broadening in a diffraction pattern of a distorted lattice and how this differs from that of a pristine crystal shown in Fig. 1(j).

Based on such Hosemann analysis, we proceed to analyze the influence of defectual-induced distortion on, say, the quasi-momentum conservation during an electron-phonon scattering event: *In the above-described distorted lattice, an electron, initially at a state \mathbf{k}_1 that goes into a final state \mathbf{k}'_1 after being scattered by a phonon with wave vector \mathbf{q} , transfers an amount of quasimomentum $\mathbf{k}'_1 - \mathbf{k}_1 - \mathbf{q} = \mathbf{g} + \delta\mathbf{g}$. Evidently, for a defectual-free system, $\delta\mathbf{g} = 0$, quasimomentum is conserved exactly and $\mathbf{q} = \mathbf{k}'_1 - \mathbf{k}_1 - \mathbf{g}$. In contrast, for a defectual-bearing system wherein $\delta\mathbf{g} \neq 0$, quasimomentum is no longer conserved [18,30,52] in the sense that $\mathbf{q} = \mathbf{k}'_1 - \mathbf{k}_1 - \mathbf{g} - \delta\mathbf{g}$ becomes increasingly arbitrary, especially when $\delta\mathbf{g}$ is lying in higher Brillouin zones. This is the essence of Gurvitch's interpretation of $T^n \rightarrow T^2$ feature in terms of the *breakdown of the electron-phonon momentum-conservation law* [52].*

Further insight into the electron-phonon scattering within a distorted lattice of Fig. 1(c) can be gained if the analysis of the last paragraph can be restated in terms of the electron-phonon structure factor, $S_q(\mathbf{k}'_1 - \mathbf{k}_1) = |\varphi(\mathbf{k}'_1 - \mathbf{k}_1 - \mathbf{q})|^2$, when written in terms of the phase of electron-phonon interaction, $\varphi(\mathbf{k}'_1 - \mathbf{k}_1 - \mathbf{q}) = (1/\sqrt{N}) \sum_{\mathbf{r}} e^{i(\mathbf{k}'_1 - \mathbf{k}_1 - \mathbf{q}) \cdot \mathbf{r}}$ (N is the

number of ions) [67]. For a pristine lattice, $S_{\mathbf{q}}(\mathbf{k}'_1 - \mathbf{k}_1) = \sum_{\mathbf{g}} \delta_{\mathbf{k}'_1 - \mathbf{k}_1 - \mathbf{q}, \mathbf{g}}$ is a sum of normal, $\mathbf{g} = (0, 0, 0)$, and Umklapp, $\mathbf{g} \neq (0, 0, 0)$, scatterings. As that, in a perfect crystal, the low-temperature ions deformation is smooth and of long wavelength (small \mathbf{q}), one usually retains only the normal events and, as a result, only longitudinal phonon modes with a well defined polarization, $\hat{\mathbf{e}}(\mathbf{q} = \mathbf{k}'_1 - \mathbf{k}_1)$, are excitable. In contrast, in a defectal-bearing distorted lattice, the electron-phonon structure factor acquires broadened features at $\mathbf{g} \neq 0$ because distortions provide a source of short wavelength (large \mathbf{q}) phase interference [18,30]. Within the framework of the distorted lattice, these features are intrinsic, as one can verify by looking at the averaged structure factor (calculated in SM1) [41]

$$\bar{S}_{\mathbf{q}}^{\ell}(\mathbf{k}'_1 - \mathbf{k}_1) \approx \delta_{\mathbf{k}'_1 - \mathbf{k}_1 - \mathbf{q}, 0} + \sum_{\mathbf{g} \neq 0} \frac{S_{\max}(\mathbf{g})}{1 + \ell_{hkl}^2 (\mathbf{k}'_1 - \mathbf{k}_1 - \mathbf{q} - \mathbf{g})^2}. \quad (4)$$

The peak amplitudes in Eq. (4) are $S_{\max}(\mathbf{g}) = 4/\sigma^2 \mathbf{g}^2 = a_o^2/\sigma^2 \pi^2 (h^2 + k^2 + l^2)$, while the Lorentzian linewidths, $\ell_{hkl} \equiv |\delta \mathbf{g}|^{-1} = 4/\sigma^2 \mathbf{g}^2 a_o = a_o/\sigma^2 \pi^2 (h^2 + k^2 + l^2) = \ell/(h^2 + k^2 + l^2)$, with $\ell = a_o/\sigma^2 \pi^2$, are inversely proportional to the widths of its peaks, $\delta \mathbf{g}$ [42]. Since now $\mathbf{k}'_1 - \mathbf{k}_1 - \mathbf{q} - \mathbf{g} \neq 0$, multiple phonon modes [longitudinal and transverse, of all polarizations $\hat{\mathbf{e}}(\mathbf{q} \neq \mathbf{k}'_1 - \mathbf{k}_1 - \mathbf{g})$] become kinematically involved: Multiple phonon modes will be available for mediating e-e scattering.

2. Softening: Lifshitz's resonance

Next we elaborate on the notion of a *heavy scatterer* or a Lifshitz's resonance [68]. Each one of such a large collection of misplaced and/or implanted atoms (being part of a defectal) can also be seen, from the point of view of long wavelength phonon waves, as a heavy scatterer. This leads to a slowing down of long wavelength vibrations and to an important transfer of spectral weight towards the lower edge of the spectrum. If the amplitude of the incident and scattered phonon waves are $\varphi_{\mathbf{q},\nu}^{(i)}$ and $\varphi_{\mathbf{q},\nu}^{(s)}$ [68], respectively, then these two quantities are related by

$$\varphi_{\mathbf{q},\nu}^{(s)} = \frac{1}{1 - \varepsilon D(\omega)} \varphi_{\mathbf{q},\nu}^{(i)}, \quad (5)$$

where $g_{\mathbf{k}',\mathbf{k},\mathbf{q},\nu} = \alpha(\omega_{\mathbf{q},\nu}) \hat{\mathbf{e}}(\mathbf{q}, \nu) \cdot (\mathbf{k}' - \mathbf{k})$ is the amplitude of the electron-phonon matrix element [including the bare $\alpha(\omega_{\mathbf{q},\nu})$ due to all branches, $\nu = L, T_1, T_2$, with dispersion $\omega_{\mathbf{q},\nu}$ and polarization $\hat{\mathbf{e}}(\mathbf{q}, \nu)$, see Sec. SM1] [41]. The first term is calculated in SM2 [41]. In the second term, ω_R and Γ are, respectively, the frequency and linewidth of the low-energy, quasilocalized phonon resonances associated with concentration, $n_d(\ell)$, of Lifshitz scatterers.

$\alpha^2 \mathcal{F}_{\ell}(\omega)$ of Eq. (9) summarizes, mathematically, the spectral function of our simple distorted-lattice-plus-heavy-scatterer model; it includes (i) the softening of the vibrational

where $\varepsilon = (\mathcal{M} - M)/M$, with \mathcal{M} being an effective *defect-related mass*, and $D(\omega)$ is a function of only the frequency ω . If the frequency of the driving wave lies inside the continuum of vibrations, especially at the bottom of the phonon bands, then $D(\omega) = \mathcal{R}e[D(\omega)] + i\mathcal{I}m[D(\omega)]$, and a resonance is found at a frequency ω_R given by the condition $\varepsilon \mathcal{R}e[D(\omega_R)] = 1$. Generally, the function $\mathcal{R}e[D(\omega)] \sim \omega^2$ and the effective mass \mathcal{M} is much heavier than the typical mass of the lattice ion M . Then, for sufficiently large $\varepsilon \gg 1$, the resonance frequency ($\omega_R \sim 1/\sqrt{\varepsilon}$) will be located at the low-frequency range of the spectrum [68].

The phase shift due to the phonon-wave scattering off defectals can be written as [68]

$$\Phi(\omega) = \arctan \left[\frac{\varepsilon \mathcal{I}m[D(\omega)]}{1 - \varepsilon \mathcal{R}e[D(\omega)]} \right], \quad (6)$$

which, when close to ω_R , changes rapidly from 0 to π , indicating that the effective impurity oscillates out of phase with respect to the underlying lattice ions. This acts as a driving force that produces the sharp resonance peak in the vibrational density of states $\mathcal{F}(\omega)$. For a concentration n_d of defectals, containing n_d defects, this peak is given by

$$\delta \mathcal{F}_R(\omega) = \frac{3}{\pi} \frac{d\Phi}{d\omega} \approx \frac{n_d}{2\pi} \frac{\Gamma}{(\omega - \omega_R)^2 + \frac{1}{4}\Gamma^2}, \quad (7)$$

and the width Γ of the resonance at ω_R is given in terms of the phase shift $\Phi(\omega)$, during the scattering of phonon waves off a dilute concentration n_d as

$$\Gamma = \frac{2\pi \mathcal{F}(\omega_R)}{\{d\Phi(\omega)/d\omega\}_{\omega_R}}. \quad (8)$$

As we can see, the larger the mass \mathcal{M} , the lower the frequency ω_R , since $\omega_R \sim 1/\sqrt{\varepsilon}$, and the sharper the resonance will be, as Γ is proportional to $\mathcal{F}(\omega_R)$ [68].

3. Combining distortions and softening

A combination of the distortion-broadened structure factor [Eq. (4)] and the quasilocalized phonon modes lead to the following generalized Eliashberg's spectral function:

$$\alpha^2 \mathcal{F}_{\ell}(\omega) = \sum_{\{\mathbf{k}', \mathbf{k}\} = \mathbf{k}_F, \mathbf{q}, \nu} \bar{S}_{\mathbf{q}}^{\ell}(\mathbf{k}' - \mathbf{k}) |g_{\mathbf{k}', \mathbf{k}, \mathbf{q}, \nu}|^2 \left\{ \delta(\omega - \omega_{\mathbf{q}, \nu}) + n_d(\ell) \frac{2}{\pi} \frac{\Gamma}{4(\omega - \omega_R)^2 + \Gamma^2} \right\}, \quad (9)$$

spectrum, through the continuous transfer of spectral weight, tracked by ℓ , from high, ω_D , to low, ω_R , frequencies, (ii) the new phonon branches, ν , and polarizations, $\hat{\mathbf{e}}(\mathbf{q}, \nu)$, through $\sum_{\mathbf{q}, \nu}$, and (iii) the sum of all kinematically unconstrained wave vectors, \mathbf{k}' , \mathbf{k} , \mathbf{g} , and \mathbf{q} ($0 \leq |\mathbf{q}| \leq 2k_F$), whose rules of momentum transfer are controlled by $\bar{S}_{\mathbf{q}}^{\ell}(\mathbf{k}' - \mathbf{k})$. We calculated $\alpha^2 \mathcal{F}_{\ell}(\omega)$ within the Debye model for phonons interacting with nearly free electrons, see SM2 [41]: Its evolution, calculated for different values of ℓ , is shown in Fig. 5(g).

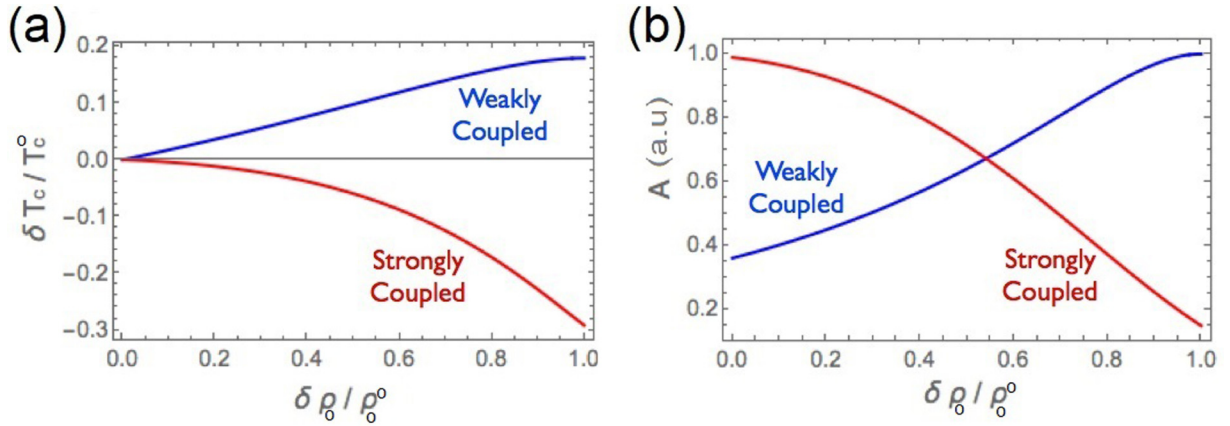


FIG. 4. Trend of calculated evolution of $T_c(\rho_o)$ and $A(\rho_o)$. Correlated variations of $\delta T_c(\delta\rho_o/\rho_o^\circ)/T_c^\circ$ [left, (a)] and $A(\delta\rho_o/\rho_o^\circ)$ [right, (b)] for the two classes of conventional superconductors considered in this work: strongly-coupled superconductors (red, decreasing) and weakly-coupled superconductors (blue, increasing). Recall that $\frac{\delta\rho_o}{\rho_o^\circ} = \frac{\lambda_\ell}{\delta\ell}$ in Eq. (2).

B. Surge and correlation of superconductivity and FL transport

We consider here the two-particle process, shown in Figs. 1(e), 1(g), and 1(i), wherein electrons, initially at states \mathbf{k}_1 and \mathbf{k}_2 , scatter—within the defectal region—into final states \mathbf{k}'_1 and \mathbf{k}'_2 by exchanging all kinematically unconstrained phonon modes \mathbf{q} with a nonzero spectral weight. The resulting retarded, attractive e-e interaction reads

$$V_{\mathbf{k}'_1, \mathbf{k}_1, \mathbf{k}'_2, \mathbf{k}_2}(\mathbf{q}, \ell) \approx -\phi_{\mathbf{q}}(\mathbf{k}'_1, \mathbf{k}_1, \mathbf{k}'_2, \mathbf{k}_2)V_{ee}(\ell). \quad (10)$$

This fully expounds the role of distortions and softening through both the phase, $\phi_{\mathbf{q}}(\mathbf{k}'_1, \mathbf{k}_1, \mathbf{k}'_2, \mathbf{k}_2) = (1/N)\sum_{\mathbf{r}} e^{i(\mathbf{k}'_1 - \mathbf{k}_1 - \mathbf{q}) \cdot \mathbf{r}} \sum_{\mathbf{r}'} e^{i(\mathbf{k}'_2 - \mathbf{k}_2 + \mathbf{q}) \cdot \mathbf{r}'}$, and amplitude, $V_{ee}(\ell)$, obtained after averaging over Fermi and Debye surfaces.

1. $T_c(\ell)$ from Eliashberg's theory

The influence of distortion and softening on $T_c(\ell)$ is analyzed in SM3 [41], giving

$$T_c(\ell) = \theta e^{-(1+\lambda_\ell)/(\lambda_\ell - \mu^*)} \quad \text{with} \quad \theta = \frac{1.13\hbar\omega_c}{k_B}, \quad (11)$$

where $\lambda_\ell = N(\epsilon_F)V_{ee}(\ell)$ and $\mu = N(\epsilon_F)V_C$ (with the pseudopotential itself being renormalized as $\mu^* = \mu/(1 + \mu \ln(\epsilon_F/\omega_c))$) [69,70]. The strength of T_c is dominantly controlled by $V_{ee}(\ell)$ since $N(\epsilon_F)$, ω_c , and μ^* are not expected to be influenced by defectal incorporation [71]. $V_{ee}(\ell)$ is highly sensitive to *softening*, namely, to shifts in spectral weight relative to an optimal frequency ω_{opt} , Figs. 5(g) and 5(h). This explains the empirical findings that T_c can be controlled by parameters such as defectal incorporation or physical/chemical pressure.

According to the scaling theorem of Coombes and Carbotte [72], when the total integrated area under the spectral function, $\alpha^2\mathcal{F}_\ell(\omega)$ in Eq. (9) and Fig. 5(g), is equal to a constant \mathcal{A} , then the best shape that maximizes T_c is a δ function (here, introduced as an Einstein spectrum). Then, in order to model the softening that clearly occurs due to distortion, see for example Fig. 5(g); we follow Combes and Carbotte [72] and replace our calculated Eliashberg's spectral function by an Einstein spectrum with distortion dependent

Einstein frequency, as described below:

$$\alpha^2\mathcal{F}_\ell(\omega) = \mathcal{A}\delta(\omega - \omega_E(\ell)),$$

$$\omega_E(\ell) \approx \omega_E(\infty) + \frac{1}{k_F\ell}[\omega_R - \omega_E(\infty)], \quad (12)$$

for $k_F\ell \gg 1$, $\omega_E(\infty) \gg \omega_R$ and $\omega_E(\infty)$ is an average phonon frequency calculated self-consistently in terms of the defectal-free $\alpha^2\mathcal{F}_\infty(\omega)$. $\omega_E(\ell)$ is monotonically decreased whenever ℓ is lowered towards a_o : Such softening was reported in disordered [30] and amorphous metals [8,18]. The evolution of the normalized λ_ℓ , undergoing such a softening, is

$$\frac{\delta\lambda_\ell}{\lambda_\infty} \approx \frac{1}{k_F\ell} \left[\frac{\omega_E^2(\infty)}{\omega_{\text{opt}}^2 + \omega_E^2(\infty)} \left(2 - \frac{1}{2k_F\ell} \right) - 1 \right] \quad (13)$$

wherein both $\omega_E(\ell)$ and ω_{opt} are much higher than the resonance frequency ω_R , see Figs. 5(g) and 5(h). The evolution of the corresponding $T_c(\ell)$ is shown in Fig. 4(a) for the following two classes of conventional superconductors.

a. Weakly coupled superconductors. A defectal-free member of this class is characterized by $\omega_E(\infty) \gg \omega_{\text{opt}}$, ω_R ($\lambda_\infty < 1$ and a relatively low T_c°). Incorporation of defectals decreases ℓ and leads, via Eq. (12), to a downwards shift of $\omega_E(\ell)$ towards ω_{opt} . This, based on the structure of $V_{ee}(\omega_E/\omega_{\text{opt}})$ of Fig. 5(g), leads to an *enhancement* [30,73] of both λ_ℓ and $T_c(\ell)$ [see Fig. 4(a)(blue)]: This explains the evolution of $T_c(\rho_o)$ in the first quadrant of Figs. 2(a)–2(c). Furthermore, for weak but positive $\frac{\delta\rho_o}{\rho_o^\circ}$, one arrives at [see Eqs. (11), (13)]

$$\frac{\delta T_c(\delta\rho_o/\rho_o^\circ)}{T_c^\circ} \approx \frac{\lambda_\infty}{(\lambda_\infty - \mu^*)} \frac{1}{k_F\ell_o} \left(\frac{\delta\rho_o}{\rho_o^\circ} \right) \implies \frac{\delta T_c}{T_c^\circ} \propto \frac{\delta\rho_o}{\rho_o^\circ}; \quad (14)$$

a linear evolution valid within the weak defectal-concentration range [26]. Indeed, this is consistent with the initial linearity of the curves in Figs. 2(a)–2(c), the experiments of, e.g., Refs. [8,22,26] and the theory of Ref. [35]. In particular, the fact that the slope in Eq. (14) is material dependent is in excellent agreement with the finding of Ref. [22].

b. Strongly coupled superconductors. A defectal-free member of this class is characterized by $\omega_R \ll \omega_E(\infty) \lesssim \omega_{\text{opt}}$ ($\lambda_\infty \gtrsim 1$ and a relatively high T_c°). Incorporation of defectals

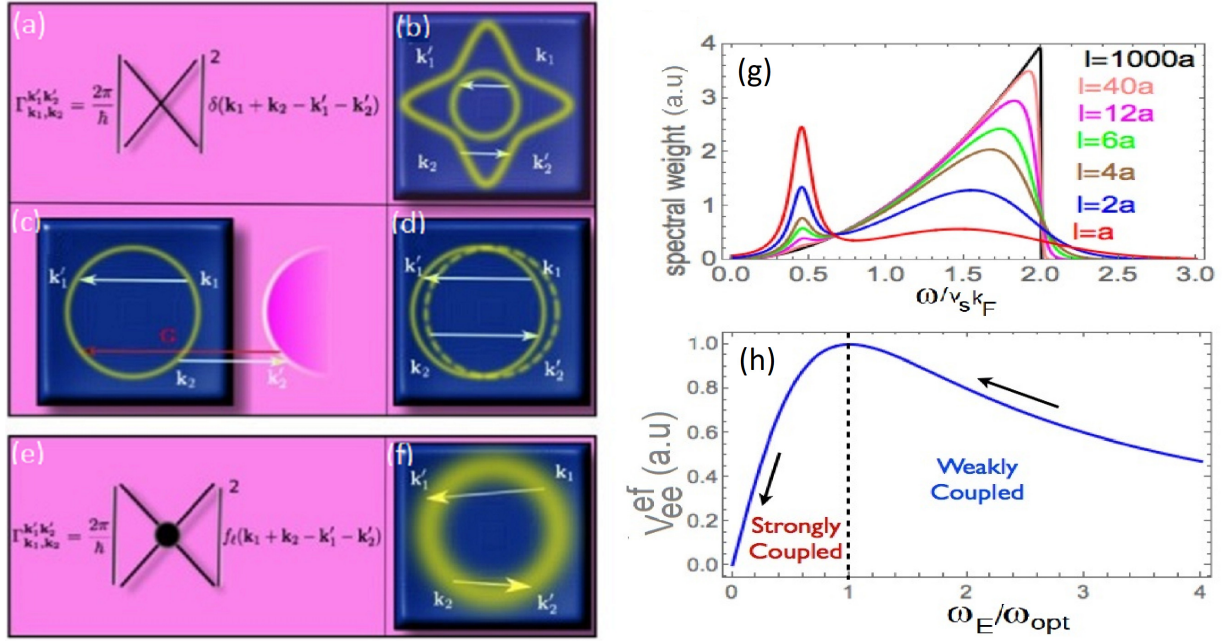


FIG. 5. Comparison of the pseudo-Umklapp channel with the traditional e-e channels and the evolution of both $\alpha^2\mathcal{F}(\omega/v_s k_F)$ and $V_{ee}(\omega_E/\omega_{opt})$. (a) $\Gamma_{\mathbf{k}_1, \mathbf{k}_2}^{\mathbf{k}'_1, \mathbf{k}'_2}$ of a defect-free system which may be under any of the following kinematically constrained scattering processes: (b) multiband or Baber scattering [74]; (c) multizone or Umklapp scattering [75,76]; (d) multisheet or topological scattering [77]. (e) $\Gamma_{\mathbf{k}_1, \mathbf{k}_2}^{\mathbf{k}'_1, \mathbf{k}'_2}$ of a defect-bearing system. (f) The kinematically unconstrained, pseudo-Umklapp relaxation channel. (g) Eliashberg's spectral function, $\alpha^2\mathcal{F}$, in terms of $\omega/v_s k_F$ for different values of ℓ , showing the transfer of spectral weight from high to low frequencies. (h) Effective e-e, V_{ee} , interaction as a function of ω_E/ω_{opt} , showing the defectual-incorporation-induced phonon softening and the flow towards lower frequencies (as indicated by the black arrows). This leads to an increase in the interaction for soft superconductors and a decrease for hard ones. It is worth mentioning that although the analysis of Figs. 2–4 emphasizes the distinct difference among the two hard and soft superconducting limits, panel (h) indicates that starting from any initial superconducting target (not necessarily a limit case), defectual-incorporation leads to a flow from weak to strong coupling (if target is above ω_{opt}) or from strong to weak limit (if target is below ω_{opt}).

shifts $\omega_E(\ell)$ downwards, away from ω_{opt} but in the direction of ω_R . This, based on the structure of $V_{ee}(\omega_E/\omega_{opt})$ of Fig. 5(h), indicates a *reduction* of $T_c(\ell)$ [30,73]: consistent with the results of the fourth quadrant of Fig. 2(a). Furthermore, for weak but positive $\frac{\delta\rho_o}{\rho_o^\circ}$, Eqs. (11) and (13) indicate that

$$\frac{\delta T_c(\delta\rho_o/\rho_o^\circ)}{T_c^\circ} \approx -t_1 \left(\frac{\delta\rho_o}{\rho_o^\circ} \right) - t_2 \left(\frac{\delta\rho_o}{\rho_o^\circ} \right)^2, \quad (15)$$

with $t_1 = (\lambda_\infty^{-1}/k_F \ell_o)(1 - 2\omega_E^2(\infty)/(\omega_{opt}^2 + \omega_E^2(\infty)))$ [which is positive for $\omega_E(\infty) \lesssim \omega_{opt}$] and a reasonably large value for $t_2 = (\lambda_\infty^{-1}/8k_F \ell_o)\omega_E^2(\infty)/(\omega_{opt}^2 + \omega_E^2(\infty)) > 0$. This shows a deviation from linearity which is consistent with the evolution of $T_c(\rho_o)$ of the fourth quadrant of Fig. 2(a), see also Fig. 4(a)(red).

2. $A(\ell)$ from Boltzmann's transport theory

It is evident from SM4 [41] that in a defect-free system, the condition $f_\infty(\mathbf{k}_1 + \mathbf{k}_2 \rightarrow \mathbf{k}'_1 + \mathbf{k}'_2) = \delta_{\mathbf{k}_1 + \mathbf{k}_2, \mathbf{k}'_1 + \mathbf{k}'_2}$ restricts severely the availability of phase space for net momentum transfer to the lattice. This is most evident for the following traditional scattering channels [Figs. 5(b)–5(d)]: (i) the Baber mechanism, for a multiband Fermi surface [74]; (ii) the Umklapp mechanism, for Fermi surfaces that are at least quarter filled [75,76]; (iii) the normal mechanism, for multiply connected Fermi surfaces with an infinite number of

self-intersecting points [77]. Then, due to that restriction, any allowed $A_\infty T^2$ contribution is typically very small (low scattering efficiency) or even vanishes identically for topologically trivial, single band, small Fermi surfaces.

The extreme specificity of these three relaxations is in stark disagreement with the ubiquity and robustness of the FL transport of defectual-bearing systems (see, e.g., Fig. 3). Indeed, Eq. SM26 of SM4 [41] indicates that the e-e structure factor $f_\ell(\mathbf{k}_1 + \mathbf{k}_2 \rightarrow \mathbf{k}'_1 + \mathbf{k}'_2) \neq \delta_{\mathbf{k}_1 + \mathbf{k}_2, \mathbf{k}'_1 + \mathbf{k}'_2}$ and, moreover, the evolution of $\rho_{ee}(T, \ell)$ exhibit a nontrivial *quadratic-in-T* character:

$$\rho_{ee}(T, \ell) = A(\ell)T^2 = [F_\ell^2 |V_{tot}(\ell)|^2]T^2, \quad (16)$$

wherein $A(\ell)$, Eq. SM37 [41], depends on the total e-e interaction, $V_{tot}(\ell) (\equiv \frac{V_c - V_{ee}(\ell)}{1 + \lambda_\ell})$ in Eq. SM31), and the efficiency of momentum relaxation, F_ℓ (Eq. SM38) [41]. Equation (16) indicates a robust FL contribution which, as mentioned before, is driven by the pseudo-Umklapp scattering process whereby the enlargement of the available phase space for quasimomentum relaxation stems from the monotonically increasing broadening of the Bragg reflections at higher-order reciprocal lattice points. Eventually, at the amorphous limit, this broadening merges into a *halo-shaped* diffraction pattern as the one shown in Fig. 1(k), Fig. 5(e), and Ref. [18]. Let us now analyze $A(\ell)$ of the two classes of defectual-bearing conventional superconductors.

3. $A(\ell)$ for weak- and strong-coupled superconductors

It is recalled that, due to the defect-induced relaxation of the kinematic constraints, all electrons lying within the Fermi surface would be involved; then, $A(\ell)$ of SM4 [41] becomes

$$A(\ell) \propto \frac{\sum_{\mathbf{k}_i, i=1\dots 4}}{|\sum_{\mathbf{k}}|^2} \rightarrow N^2(\epsilon_F). \quad (17)$$

Moreover, on approaching the superconducting instability from the FL side, $V_{\text{tot}}(\ell)$ is renormalized [see Eq. (SM31)] [78]. Then,

$$A_\ell \propto N(\epsilon_F)^2 |V_{\text{tot}}(\ell)|^2 = F_\ell^2 \left(\frac{\lambda_\ell - \mu^*}{1 + \lambda_\ell} \right)^2. \quad (18)$$

Within the range of long ℓ and $1 \ll k_F \ell_p < \infty$, Eq. (18) can be expanded around λ_∞ , as

$$A_\ell(\delta\lambda_\ell) \simeq A_\infty + a_1(\delta\lambda_\ell) + a_2(\delta\lambda_\ell)^2, \quad (19)$$

where A_∞ is the negligibly small kinematically constrained contributions from the host matrix, while the second and third terms, with $a_1 = 2(|\lambda_\infty - \mu^*|(1 + \mu^*)/(1 + \lambda_\infty)^3)$ and $a_2 = (1 + \mu^* - 2|\lambda_\infty - \mu^*|)(1 + \mu^*)/(1 + \lambda_\infty)^4$, include contributions from all kinematically unconstrained relaxation processes.

Equation (19) is not suitable for a direct comparison with experiments; rather, as seen in Figs. 3(a8) and 3(b1), it is advantageous to express A in terms of ρ_o . This can be straightforwardly established by employing $\delta\lambda \propto \delta\rho_o$ (see note [79]). Alternatively, we proceed by recalling that in a typical FL, the frequency dependence of the imaginary part of the self-energy is given by $\text{Im}\Sigma(\omega) \sim \omega^2$. Then, on considering the relevant energy scale to be set by $k_B T$, one obtains the characteristic FL *quadratic-in-T* resistivity [80]. In contrast, at $T = 0$ limit, the relevant energy scale in a disordered system is set by the *fuzziness* of the Fermi surface ($\delta\mathbf{g} \neq \mathbf{0}$ or $\sigma \neq \mathbf{0}$ in the Hosemann's paracrystalline structure) which is driven by the spatially and randomly distributed defectals. This, together with the analysis of Eq. (4), suggests that $\rho_o \propto \ell^{-1} \propto \frac{\sigma^2 \pi^2}{a_o}$: This establishes a correlation among ρ_o and each of $T_c(\ell)$ and $A(\ell)$. Guided by these considerations, as well as Eq. (19) and the empirical relation deduced from Figs. 3(a8) and 3(b1), one obtains

$$A(\ell) \simeq A_o + A_1(\rho_o) + A_2(\rho_o)^2, \quad (20)$$

where $A_i (i = 0, 1, 2)$ are functions of F_ℓ^2 , μ^* , and λ_∞ [81]. Calculated trends of $A(\rho_o)$, based on Eq. (20), are plotted in Fig. 4(b): The red line represents the evolution of a defectal-bearing strongly coupled superconductor while the blue line that of a distorted weakly coupled superconductor. A fit of Eq. (20) to the $A(\rho_o)$ curve of neutron-irradiated V_3Si strong-coupled superconductor [9], shown in Fig. 3(a8), gives $A = .0027 - 1.71 \times 10^{-5} \rho_o - 6.67 \times 10^{-8} \rho_o^2 \mu\Omega \text{ cm K}^{-2}$. Similarly, a fit of Eq. (20) to the data of weak-coupled In thin-film superconductor [2], shown in Fig. 3(b1), gives $A = 0.095 + 0.0075 \rho_o^2 \mu\Omega \text{ cm K}^{-2}$. All ρ_o values are in $\mu\Omega \text{ cm}$.

C. Universal scaling law between $T_c(\ell)$ and $A(\ell)$ in defectal-bearing superconductors

The correlation of T_c and A is obtained after combining the expressions of $A(\ell)$ [Eq. (18)] and $T_c(\ell)$ [Eq. (11)]:

$$T_c(\ell) = 1.13 \frac{\hbar\omega_c}{k_B} e^{-(1+\lambda_\ell)/(\lambda_\ell - \mu^*)} = \theta e^{-F_\ell/\sqrt{A_\ell}}, \quad (21)$$

wherein F_ℓ is given in Eq. (SM38) [41]. Within the studied experimental ranges, both F_ℓ and θ are assumed to be hardly influenced by temperature or defectal incorporation. It is assuring that all the studied superconductors, see Fig. 3(c), obey the scaling of Eq. (21), namely those with intentional defectal incorporation. The ranges of θ and F_ℓ can be illustrated by the fit parameters of V_3Si : $\theta \approx 45 \text{ K}$ and $F_\ell \approx 0.004 (m\Omega)^{1/2} \text{ cm}^{1/2} \text{ K}^{-1}$.

Within the spirit of the renormalization group, defectal incorporation in conventional superconductors can be seen as a relevant perturbation that promotes the running of λ_ℓ towards either the weak- or strong-coupling limits, depending on the relative values of $\omega_E(\infty)$ and ω_{opt} . For weakly coupled superconductors, where $\omega_E(\infty) \gg \omega_{\text{opt}}$ and $\lambda_\infty < 1$, the running is towards stronger coupling: This justifies the procedure used in Refs. [25,82] for calculating, via McMillan strong-coupling equation [Eq. (11)] [69,70], the maximum T_c of soft superconductors such as Al, Zn, and Sn. On the other hand, for the strongly coupled superconductors, with $\omega_E(\infty) \lesssim \omega_{\text{opt}}$ and $\lambda_\infty \gtrsim 1$, the running is towards weaker couplings: This explains the finding, in Refs. [19–21,56], of a universal trend of T_c versus resistivity ratio of hard superconductors such as Nb and A-15. Based on Eq. (21), we conclude that the incorporation of defectals promotes the *correlated flow* of $T_c(\ell)$ and $A(\ell)$, *without ever leaving the curve plotted in Fig. 3(c)*.

IV. DISCUSSIONS, SUMMARY, AND OUTLOOK

The generalization of our approach to the analysis of other properties can be demonstrated by calculating the Kadowaki-Woods ratio and the gap-to- T_c ratio of defectal-bearing conventional superconductors. Below we show that a strong variation in these two parameters can be observed if distortion and softening are introduced.

The Kadowaki-Woods ratio is defined as A/γ^2 and is expected to be a universal constant in FLs since $A \propto m^{*2}$ and $\gamma \propto m^*$. Based on the ratio expressions reported for transition-metal-based [83] or heavy-fermion [47] materials, we calculate the defectal-related Kadowaki-Woods ratio to be modified by a geometric multiplication factor F_ℓ^2/F_∞^2 :

$$\begin{aligned} \frac{A(\ell)}{\gamma^2} &= \left(\frac{F_\ell^2}{F_\infty^2} \right) \frac{81}{4\pi \hbar k_B^2 e^2} \frac{1}{d^2 n N^2(\epsilon_F) \langle v_{\text{ox}}^2 \rangle} \\ \Rightarrow \frac{\left(\frac{A(\ell)}{\gamma^2} \right)}{\left(\frac{A(\infty)}{\gamma^2} \right)} &= \frac{F_\ell^2}{F_\infty^2}, \end{aligned} \quad (22)$$

where $\langle v_{\text{ox}}^2 \rangle$ is a Fermi surface average of the carrier velocity squared that accounts for anisotropies, e is the electric charge of the direct, Coulomb, electric-electric interaction, n is the carrier density, and $d \sim 1$ is a dimensionless number [83]. As we have discussed earlier, F_ℓ^2/F_∞^2 is a measure of the efficiency of momentum relaxation via pseudo-Umklapp

scattering process (due to the induced easing of kinematic constraints, $F_\ell^2 > F_\infty^2$).

Based on the analysis of Ref. [72], the gap-to- T_c ratio of a defect-bearing superconductor, within the $T_c/\theta \ll 1$ range, is approximated as

$$\begin{aligned} \frac{2\Delta(\ell)}{k_B T_c(\ell)} &\approx 3.53 \left(1 + 12.5 \left[\frac{T_c(\ell)}{\theta} \right]^2 \ln \left[\frac{\theta}{2T_c(\ell)} \right] \right) \\ \Rightarrow \frac{\left(\frac{2\Delta(\ell)}{k_B T_c(\ell)} \right)}{\left(\frac{2\Delta(\infty)}{k_B T_c(\infty)} \right)} &\approx \frac{1 + 12.5 \left[\frac{T_c(\ell)}{\theta} \right]^2 \ln \left[\frac{\theta}{2T_c(\ell)} \right]}{1 + 12.5 \left[\frac{T_c(\infty)}{\theta} \right]^2 \ln \left[\frac{\theta}{2T_c(\infty)} \right]} \end{aligned} \quad (23)$$

which, in satisfactory agreement with the empirical findings of Ref. [26], indicates that—for weakly-coupled superconducting defect-free simple metals—the gap-to- T_c ratio is the universal ratio $2\Delta(\infty)/k_B T_c(\infty) = 3.53$. As defectals are incorporated, this ratio increases with $T_c(\ell)$, showing that the flow is towards stronger couplings. The opposite occurs for the case of defect-free, strongly coupled, superconductors, where $2\Delta(\infty)/k_B T_c(\infty) = 3.53\{1 + 12.5[T_c(\infty)/\theta]^2 \ln[\theta/2T_c(\infty)]\} > 3.53$. But, as defectals are incorporated, $T_c(\ell)$ decreases while this ratio decreases, towards the universal ratio of 3.53, showing that the flow is towards weaker couplings.

Finally, the universality of the above mentioned exotic effects can be gauged from the extensive experimental (see, e.g., compiled data in Figs. 2 and 3, Refs. [11,13,15,17,19,53,84–86] and references therein) as well as theoretical (e.g., Refs. [18,30,34–40] and references therein) studies. Our theoretical approach is successfully applied to the analysis of these effects which emerge from all metallic thin films wherein “stabilized defect complexes” are incorporated. Nevertheless, our analysis is not applicable to any defective, but defectal-nonbearing, superconductor that exhibits (i) superconductivity in annealed defective samples wherein segregated single isolated, granular (nano-)structured defects emerge [87], including as well annealed soft superconductors exhibiting a weak drop in T_c for doping below 1% [88], (ii) superconductivity within multilayered structures wherein metal-metal or metal-insulator effects are dominant [15], (iii) superconductivity in material with activated normal-state conductivity [15,86], (iv) superconductivity at cavities [15], (v) superconductivity in H(D)-implanted transition metals wherein anharmonicity or negative isotope effects are dominant [19,53], and (vi) superconductivity involving one or two dimensions or ultrathin films wherein surface or size quantization effects enter into consideration [15]. It is worth emphasizing that, in contrast to this limited list of excluded systems, our analysis is suitable for rationalizing the aforementioned wide class of defectal-bearing superconductors. Preliminary analysis indicates that it can be extended to the following list of highly possible candidates: magnesium diboride MgB_2 (a strong-coupled superconductor that shows a correlation among T_c and A) [64], the perovskite titanate $\text{SrTiO}_{3-\delta}$ (exhibiting a correlated superconductivity and AT^2 contribution within a wide temperature range) [89,90], the conventional high T_c sulphur hydride H_2S superconductor [91], the irradiated $\text{La}_{1.875}\text{BaCuO}_4$ perovskite [10] as well

as the broader class of overdoped, high- T_c , superconducting cuprates (revealing a FL regime close to the superconducting state) [84,85,92,93].

In summary, we analyzed, empirically, the surge and correlation of superconductivity and FL transport of defectal-bearing conventional superconductors [shown in the first and fourth quadrants of Fig. 2(a)]. We also showed, though briefly, that these features are evident as well in other nontraditional defect-bearing superconductors such as the ones shown in the second quadrant (irradiated semiconducting-based alloys) and those in the third quadrant (the pnictides, the chalcogenides, and the heavy fermion superconductors). Theoretically, after modeling the lattice distortion in terms of Hosemann’s paracrystalline structure and using standard quantum many-body techniques, we demonstrated that the influence of both distortion and softening leads to a surge of the pseudo-Umklapp scattering channel. We derived expressions that describe the evolution of the superconductivity, the FL state, and their universal scaling correlation. We showed that these analytical expressions are in satisfactory agreement with the experimental data. Finally, limitation of our analysis as well as its extension to other defect-bearing superconductors are also outlined.

V. METHODS

The experimental data analyzed in this work were collected from the extensively reported literature on the influence of disorder on superconductivity, FL character, and residual resistivity. The experimental methods, techniques, and analysis used for obtaining the original data were detailed in the cited literature. Here, we measure the extent of defectal-incorporation in terms of the ratio of the residual resistivities $\frac{\delta\rho_s}{\rho_s^0}$. On the other hand, the extent of its influence on the superconductivity is probed in terms of the evolution of $\frac{\delta T_c}{T_c}$ while that of the Fermi liquid character is in terms of the evolution of A . The correlation among superconductivity and FL state is demonstrated in terms of the log-log plot of T_c vs $A^{\frac{1}{2}}$. For the theoretical analysis, we made use of standard quantum many-body techniques and the description of defectals in terms of Hosemann’s paracrystal supplemented by a Lifshitz resonance. All superconducting properties were calculated within the formalism of electron-phonon superconductivity according to Eliashberg’s theory, where the effects of softening are most relevant for the evolution of T_c . For the analysis of FL resistivity, we used low-temperature Boltzmann’s quantum transport theory for a distorted lattice, where distortion is the most relevant ingredient for enlarging the phase space for momentum relaxation. Our calculations include both weakly and strongly coupled regimes at low temperature and arbitrary strength of disorder.

ACKNOWLEDGMENTS

We are grateful to Pedro B. Castro and Davi A. D. Chaves for their assistance in the literature search and experimental data analysis during the initial stage of this project. We are also grateful to Indranil Paul and Eduardo Miranda for numerous and fruitful discussions.

- [1] P. Ehrhart, in *Landolt-Bornstein, New Series III*, Vol. 25 (Springer, Berlin, 1991), Chap. 2, p. 88.
- [2] G. Heim, W. Bauriedl, and W. Buckel, *J. Nucl. Mater.* **72**, 263 (1978).
- [3] O. Meyer, *Radiat. Eff.* **48**, 51 (1980).
- [4] E. H. C. P. Sinnecker, M. M. Sant'Anna, and M. ElMassalami, *Phys. Rev. B* **95**, 054515 (2017).
- [5] A. Lamoise, J. Chaumont, F. Meunier, and H. Bernas, *J. Phys., Lett.* **36**, 271 (1975).
- [6] A. Lamoise, J. Chaumont, F. Lulu, F. Meunier, and H. Bernas, *J. Phys., Lett.* **37**, 287 (1976).
- [7] F. Meunier, P. Pfeuty, A. Lamoise, J. Chaumont, H. Bernas, and C. Cohen, *J. Phys., Lett.* **38**, 435 (1977).
- [8] P. Ziemann, O. Meyer, G. Heim, and W. Buckel, *Z Physik B* **35**, 141 (1979).
- [9] R. Caton and R. Viswanathan, *Phys. Rev. B* **25**, 179 (1982).
- [10] M. Leroux, V. Mishra, J. P. Ruff, H. Claus, M. P. Smylie, C. Opagiste, P. Rodière, A. Kayani, G. Gu, J. M. Tranquada *et al.*, *Proc. Natl. Acad. Sci. USA* **116**, 10691 (2019).
- [11] B. Abeles, P. Sheng, M. Coutts, and Y. Arie, *Adv. Phys.* **24**, 407 (1975).
- [12] J. J. Hauser, *Phys. Rev. B* **3**, 1611 (1971).
- [13] G. Deutscher, in *Superconductivity*, edited by K. Bennemann and J. Ketterson (Springer, Berlin, 2008), p. 259.
- [14] F. Meunier, J. Hauser, J. Burger, E. Guyon, and M. Hesse, *Phys. Lett. A* **28**, 37 (1968).
- [15] M. Strongin, *Physica* **55**, 155 (1971).
- [16] A. Fontaine and F. Meunier, *Phys. Kondens. Mater.* **14**, 119 (1972).
- [17] B. Stritzker, in *Surface Modification and Alloying: by Laser, Ion, and Electron Beams*, edited by J. M. Poate, G. Foti, and D. C. Jacobson (Springer US, Boston, MA, 1983), Chap. 6, pp. 165–187.
- [18] G. Bergmann, *Phys. Rep.* **27**, 159 (1976).
- [19] H. Bernas and P. Nedellec, *Nucl. Instrum. Methods* **182-183**, 845 (1981).
- [20] L. R. Testardi, J. M. Poate, and H. J. Levinstein, *Phys. Rev. B* **15**, 2570 (1977).
- [21] G. Linker, *Radiat. Eff.* **47**, 225 (1980).
- [22] W. Miehle, R. Gerber, and P. Ziemann, *Phys. Rev. B* **45**, 895 (1992).
- [23] N. Bachar, S. Lerer, S. Hacothen-Gourgy, B. Almog, and G. Deutscher, *Phys. Rev. B* **87**, 214512 (2013).
- [24] A. Hofmann, P. Ziemann, and W. Buckel, *Nucl. Instrum. Methods* **182-183**, 943 (1981).
- [25] F. Ochmann and B. Stritzker, *Nucl. Instr. Meth. Phys. Res.* **209-210**, 831 (1983).
- [26] G. Bergmann, *Z. Physik* **228**, 25 (1969).
- [27] Another impressive example is the 300× enhancement in T_c of Be thin film: It goes from 0.026 K in nondefective pristine sample to about 9 K in the defect-bearing one (see Ref. [17]).
- [28] Using self-implanted In thin film, Heim *et al.* [2] reported the first observation of a defect-driven quadratic-in- T resistivity term. Later, Gurvitch [52] identified and correctly interpreted the T^2 contribution in strongly-coupled superconducting alloys.
- [29] W. Buckel and R. Hilsch, *Z. Physik* **131**, 420 (1952); **138**, 109 (1954), were the first to recognize (i) the correlation of T_c with ρ_o , (ii) the distinction of evolution of $T_c(\rho_o)$ of the limit, weak and strong coupled, superconductors, and (iii) the influence of annealing on T_c and ρ_o .
- [30] G. Bergmann, *Phys. Rev. B* **3**, 3797 (1971).
- [31] P. W. Anderson, *J Phys Chem Solids* **11**, 26 (1959).
- [32] A. H. MacDonald, *Phys. Rev. Lett.* **44**, 489 (1980).
- [33] We recall two exceptions: (i) T_c and A of some conventional FL superconductors can be expressed in terms of Landau parameters [65]. Then, under specific conditions, one obtains a relation similar to Eq. (21) [65]. (ii) Using the standard relation $T_c = \theta \exp(\frac{-1}{vN_{EF}})$ and assuming the Kadowaki-Woods relation and ($A \propto \gamma^2 \propto [N_{EF}]^2$), one obtains a relation similar to Eq. (21). Nevertheless, both analyses are drastically different from our approach since neither a correlation between A and ρ_o , nor between T_c and ρ_o can be obtained. In fact, Anderson theorem excludes the latter relation.
- [34] M. Baggio, C. Setty, and A. Zaccone, *Phys. Rev. B* **101**, 214502 (2020).
- [35] B. Keck and A. Schmid, *J Low Temp Phys* **24**, 611 (1976).
- [36] F. Kus and J. Carbotte, *Solid State Commun.* **29**, 715 (1979).
- [37] D. Belitz, *Phys. Rev. B* **36**, 47 (1987).
- [38] M. Howson and B. Gallagher, *Phys Rep* **170**, 265 (1988).
- [39] G. D. Mahan and Z. Wang, *Phys. Rev. B* **39**, 4926 (1989).
- [40] G. Kerker and K. Bennemann, *Z. Physik* **264**, 15 (1973).
- [41] See Supplemental Material at <http://link.aps.org/supplemental/10.1103/PhysRevB.104.014520> for a calculation of the role of defect-induced quantum interference into the electron-phonon coupling and its consequences regarding softening and kinematics.
- [42] R. Hosemann, W. Vogel, and D. Weick, *Acta Cryst.* **A37**, 85 (1981).
- [43] R. Hosemann and A. M. Hindeleh, *J. Macromol. Sci. -Phys., B* **34**, 327 (1995).
- [44] B. Stritzker, *Phys. Rev. Lett.* **42**, 1769 (1979).
- [45] U. Görlach, M. Hitzfeld, P. Ziemann, and W. Buckel, *Z Physik B* **47**, 227 (1982).
- [46] B. Stritzker and H. Wühl, *Z Physik B* **24**, 367 (1976).
- [47] M. ElMassalami, P. B. Castro, and M. B. S. Neto (unpublished).
- [48] W. Bauriedl, G. Heim, and W. Buckel, *Phys. Lett. A* **57**, 282 (1976).
- [49] G. Heim and E. Kay, *J. Appl. Phys.* **46**, 4006 (1975).
- [50] L. R. Testardi and L. F. Mattheiss, *Phys. Rev. Lett.* **41**, 1612 (1978).
- [51] F. Zawislak, H. Bernas, L. Mendoza-Zelis, A. Traverse, J. Chaumont, and L. Dumoulin, *Nucl. Instrum. Methods* **182-183**, 969 (1981).
- [52] M. Gurvitch, *Phys. Rev. Lett.* **56**, 647 (1986).
- [53] B. Stritzker, “Ion implantation—a promising technique for the production of new superconducting materials,” in *Advances in Superconductivity*, edited by B. Deaver and J. Ruvalds (Springer US, Boston, MA, US, 1983), pp. 347–386.
- [54] B. Stritzker, *Z. Physik* **268**, 261 (1974).
- [55] P. Ziemann, G. Heim, and W. Buckel, *Solid State Commun.* **27**, 1131 (1978).
- [56] H. Adrian, G. Ischenko, M. Lehmann, P. Müller, H. Braun, and G. Linker, *J. Less-Common Met.* **62**, 99 (1978).
- [57] J. M. Poate, R. C. Dynes, L. R. Testardi, and R. H. Hammond, *Phys. Rev. Lett.* **37**, 1308 (1976).
- [58] O. Meyer and G. Linker, *J Low Temp Phys* **38**, 747 (1980).
- [59] F. Ishikawa, N. Eguchi, M. Kodama, K. Fujimaki, M. Einaga, A. Ohmura, A. Nakayama, A. Mitsuda, and Y. Yamada, *Phys. Rev. B* **79**, 172506 (2009).

- [60] P. B. Castro, J. L. Ferreira, M. B. S. Neto, and M. ElMassalami, *J. Phys.: Conf. Ser.* **969**, 012050 (2018).
- [61] L. Sun, X.-J. Chen, J. Guo, P. Gao, Q.-Z. Huang, H. Wang, M. Fang, X. Chen, G. Chen, Q. Wu, C. Zhang, D. Gu, X. Dong, L. Wang, K. Yang, A. Li, X. Dai, H.-k. Mao, and Z. Zhao, *Nature (London)* **483**, 67 (2012).
- [62] A. T. Holmes, D. Jaccard, and K. Miyake, *Phys. Rev. B* **69**, 024508 (2004).
- [63] C. Soares, M. ElMassalami, Y. Yanagisawa, M. Tanaka, H. Takeya, and Y. Takano, *Sci. Rep.* **8**, 7041 (2018).
- [64] M. Nunez-Regueiro, G. Garbarino, and M. D. Nunez-Regueiro, *J Phys: Conf. Series* **400**, 022085 (2012).
- [65] D. van der Marel, J. L. M. van Mechelen, and I. I. Mazin, *Phys. Rev. B* **84**, 205111 (2011).
- [66] It is emphasized that the conclusion reached in this work would not be influenced by these illustrative structural arguments.
- [67] J. M. Ziman, *Electrons and phonons: the theory of transport phenomena in solids* (Oxford University Press, Oxford, UK, 1979).
- [68] I. M. Lifshitz and A. M. Kosevich, *Rep. Prog. Phys.* **29**, 217 (1966).
- [69] P. B. Allen and R. C. Dynes, *Phys. Rev. B* **12**, 905 (1975).
- [70] W. L. McMillan, *Phys. Rev.* **167**, 331 (1968).
- [71] Defectal incorporation in semiconductor films is expected to modify as well $N(\epsilon_F)$. On the other hand, for heavy fermions, both ω_c and μ^* are expected to be modified as well.
- [72] J. P. Carbotte, *Rev. Mod. Phys.* **62**, 1027 (1990).
- [73] G. Bergmann and D. Rainer, *Z. Physik* **263**, 59 (1973).
- [74] W. G. Baber, *Proc. R. Soc. London Ser. A* **158**, 383 (1937).
- [75] K. Yamada and K. Yosida, *Prog. Theor. Phys.* **76**, 621 (1986).
- [76] H. Maebashi and H. Fukuyama, *J. Phys. Soc. Jpn.* **67**, 242 (1998).
- [77] H. K. Pal, V. I. Yudson, and D. L. Maslov, *Lith. J. Phys.* **52**, 142 (2012).
- [78] S.-W. Tsai, A. H. Castro Neto, R. Shankar, and D. K. Campbell, *Phys. Rev. B* **72**, 054531 (2005).
- [79] Based on Eq. (5) of Ref. [26], for low defects, one obtains $\delta\lambda_\ell \propto \frac{1}{\ell} \propto \delta\rho_o$. Recall that $\delta\rho_o \equiv \rho_o - \rho_o^\circ (\approx \rho_o$ for negligible ρ_o°).
- [80] Intuitively, this is related to the fact that, for a given temperature T , $N(E_F)k_B T$ single particles within the Fermi surface are participating in the phonon-mediated two-particle channel (each single particle can scatter into one another via this scattering process): This generates the famous AT^2 resistivity contribution; specifically, our analysis showed that this channel leads to a FL state with A as in Eq. (18) and superconductivity with T_c as in Eq. (11).
- [81] Two limit contributions can be identified: (i) host contribution ($A_o > 0, A_1 \simeq 0, A_2 \simeq 0$), and (ii) Koshino-Taylor contribution ($A_1 > 0, A_o \simeq 0, A_2 \simeq 0$).
- [82] M. Strongin, O. Kammerer, J. Crow, R. Parks, D. Douglass Jr, and M. Jensen, *Phys. Rev. Lett.* **21**, 1320 (1968).
- [83] A. C. Jacko, J. O. Fjærestad, and B. J. Powell, *Nat Phys* **5**, 422 (2009).
- [84] D. M. Parkin, *Metallurgical Transactions A* **21**, 1015 (1990).
- [85] L. Rehn, *Nucl. Instrum. Methods Phys. Res., Sect. B* **64**, 161 (1992).
- [86] E. Bustarret, *Physica C: Superconductivity Applications* **514**, 36 (2015).
- [87] I. S. Beloborodov, A. V. Lopatin, V. M. Vinokur, and K. B. Efetov, *Rev. Mod. Phys.* **79**, 469 (2007).
- [88] G. Chanin, E. A. Lynton, and B. Serin, *Phys. Rev.* **114**, 719 (1959).
- [89] X. Lin, G. Bridoux, A. Gourgout, G. Seyfarth, S. Krämer, M. Nardone, B. Fauqué, and K. Behnia, *Phys. Rev. Lett.* **112**, 207002 (2014).
- [90] X. Lin, B. Fauqué, and K. Behnia, *Science* **349**, 945 (2015).
- [91] A. P. Drozdov, M. I. Erements, I. A. Troyan, V. Ksenofontov, and S. I. Shylin, *Nature (London)* **525**, 73 (2015).
- [92] D. Pines, *J. Phys. Chem. B* **117**, 13145 (2013).
- [93] W. Lang, M. Marksteiner, M. Bodea, K. Siraj, J. Pedarnig, R. Kolarova, P. Bauer, K. Haselgrübler, C. Hasenfuss, I. Beinik, and C. Teichert, *Nucl. Ins. Methods Physics Res. Sec. B: Beam Interactions Materials Atoms* **272**, 300 (2012).